Transverse spin angular momentum of tightly focused full Poincaré beams

W. Zhu,[1,2] V. Shvedov,[2] W. She,[1,*] and W. Krolikowski[2,3]

[1]*State Key Laboratory of Optoelectronic Materials and Technologies, Sun Yat-Sen University, Guangzhou 510275, China*
[2]*Research School of Physics and Engineering, The Australian National University, Canberra, ACT 0200 Australia*
[3]*Science Program, Texas A&M University at Qatar, Doha, Qatar*
[*]*shewl@mail.sysu.edu.cn*

Abstract: We show theoretically that by tightly focusing a full Poincaré beam one can create states of light whose average spin angular momentum (SAM) is purely transverse. Moreover, the transverse SAM is significantly increased if a narrow annular aperture is inserted into the Poincaré beam. In this case the state with transverse SAM can exist over an extremely long distance along the optical axis. To avoid diffraction on the aperture and increase the light conversion efficiency we employ the phenomenon of conical diffraction in biaxial crystals to convert a Gaussian beam into a ring-shaped beam, with a high ratio of the ring radius to its width.

©2015 Optical Society of America

References and links

1. F. J. Belinfante, "On the current and the density of the electric charge, the energy, the linear momentum and the angular momentum of arbitrary fields," Physica **7**(5), 449–474 (1940).
2. J. D. Jackson, *Classical Electrodynamics*, 3rd ed. (Wiley, 1999).
3. L. Allen, S. M. Barnett, and M. J. Padgett, *Optical Angular Momentum* (Institute of Physics Publishing, 2003).
4. M. V. Berry, "Optical currents," J. Opt. A, Pure Appl. Opt. **11**(9), 094001 (2009).
5. A. Bekshaev, K. Bliokh, and M. Soskin, "Internal flows and energy circulation in light beams," J. Opt. **13**(5), 053001 (2011).
6. K. Y. Bliokh and F. Nori, "Transverse and longitudinal angular momenta of light," Phys. Rep. **592**, 1–38 (2015).
7. A. Bekshaev, K. Bliokh, and F. Nori, "Transverse spin and momentum in two-wave interference," Phys. Rev. X **5**(1), 011039 (2015).
8. C.-F. Li, "Spin and orbital angular momentum of a class of nonparaxial light beams having a globally defined polarization," Phys. Rev. A **80**(6), 063814 (2009).
9. P. Banzer, M. Neugebauer, A. Aiello, C. Marquardt, N. Lindlein, T. Bauer, and G. Leuchs, "The photonics wheel- demonstration of a state of light with purely transverse angular momentum," J. Eur. Opt. Soc. **8**, 13032 (2013).
10. M. Neugebauer, T. Bauer, A. Aiello, and P. Banzer, "Measuring the transverse spin density of light," Phys. Rev. Lett. **114**(6), 063901 (2015).
11. W. Zhu and W. She, "Generation of tunable three-dimensional polarization in 4Pi focusing system," Opt. Express **21**(14), 17265–17274 (2013).
12. W. Zhu and W. She, "Transverse angular momentum and transverse barycenter shift of a focused light field due to nonuniform input angular momentum," Opt. Lett. **39**(6), 1337–1340 (2014).
13. Q. Zhan, "Cylindrical vector beams: from mathematical concepts to applications," Adv. Opt. Photonics **1**(1), 1–57 (2009).
14. V. Shvedov, P. Karpinski, Y. Sheng, X. Chen, W. Zhu, W. Krolikowski, and C. Hnatovsky, "Visualizing polarization singularities in Bessel-Poincaré beams," Opt. Express **23**(9), 12444–12453 (2015).
15. K. Youngworth and T. Brown, "Focusing of high numerical aperture cylindrical-vector beams," Opt. Express **7**(2), 77–87 (2000).
16. A. M. Beckley, T. G. Brown, and M. A. Alonso, "Full Poincaré beams," Opt. Express **18**(10), 10777–10785 (2010).
17. F. Cardano, E. Karimi, L. Marrucci, C. de Lisio, and E. Santamato, "Generation and dynamics of optical beams with polarization singularities," Opt. Express **21**(7), 8815–8820 (2013).

18. D. Colas, L. Dominici, S. Donati, A. A. Pervishko, T. C. H. Liew, I. A. Shelykh, D. Ballarini, M. de Giorgi, A. Bramati, G. Gigli, E. del Valle, F. P. Laussy, A. V. Kavokin, and D. Sanvitto, "Polarization shaping of Poincaré beams by polariton oscillations," Light Sci. Appl. **4**(11), e350 (2015).
19. Z. Chen, T. Zeng, B. Qian, and J. Ding, "Complete shaping of optical vector beams," Opt. Express **23**(14), 17701–17710 (2015).
20. C. Wei, D. Wu, C. Liang, F. Wang, and Y. Cai, "Experimental verification of significant reduction of turbulence-induced scintillation in a full Poincaré beam," Opt. Express **23**(19), 24331–24341 (2015).
21. E. J. Galvez, S. Khadka, W. H. Schubert, and S. Nomoto, "Poincaré-beam patterns produced by nonseparable superpositions of Laguerre-Gauss and polarization modes of light," Appl. Opt. **51**(15), 2925–2934 (2012).
22. N. B. Simpson, K. Dholakia, L. Allen, and M. J. Padgett, "The Mechanical equivalence of spin and orbital angular momentum of light: an optical spanner," Opt. Lett. **22**(1), 52–54 (1997).
23. M. E. J. Friese, T. A. Nieminen, N. R. Heckenberg, and H. Rubinsztein-Dunlop, "Optical alignment and spinning of laser-trapped microscopic particles," Nature **394**(6691), 348–350 (1998).
24. V. Garcés-Chávez, D. McGloin, M. J. Padgett, W. Dultz, H. Schmitzer, and K. Dholakia, "Observation of the transfer of the local angular momentum density of a multiringed light beam to an optically trapped particle," Phys. Rev. Lett. **91**(9), 093602 (2003).
25. V. Shvedov, C. Hnatovsky, N. Eckerskorn, A. Rode, and W. Krolikowski, "Polarization-sensitive photophoresis," Appl. Phys. Lett. **101**(5), 051106 (2012).
26. V. Shvedov, A. R. Davoyan, C. Hnatovsky, N. Engheta, and W. Krolikowski, "A long-range polarization-controlled optical tractor beam," Nat. Photonics **8**(11), 846–850 (2014).
27. C. Hnatovsky, V. Shvedov, W. Krolikowski, and A. Rode, "Revealing local field structure of focused ultrashort pulses," Phys. Rev. Lett. **106**(12), 123901 (2011).
28. C. Hnatovsky, V. G. Shvedov, and W. Krolikowski, "The role of light-induced nanostructures in femtosecond laser micromachining with vector and scalar pulses," Opt. Express **21**(10), 12651–12656 (2013).
29. K. Lou, S.-X. Qian, Z.-C. Ren, C. Tu, Y. Li, and H.-T. Wang, "Femtosecond laser processing by using patterned vector optical fields," Sci. Rep. **3**, 2281 (2013).
30. C. Varin, S. Payeur, V. Marceau, S. Fourmaux, A. April, B. Schmidt, P.-L. Fortin, N. Thiré, T. Brabec, F. Légaré, J.-C. Kieffer, and M. Piché, "Direct electron acceleration with radially polarized laser beams," Appl. Sci. **3**(1), 70–93 (2013).
31. T. Ehmke, T. H. Nitzsche, A. Knebl, and A. Heisterkamp, "Molecular orientation sensitive second harmonic microscopy by radially and azimuthally polarized light," Biomed. Opt. Express **5**(7), 2231–2246 (2014).
32. F. Belinfante, "On the current and the density of the electric charge, the energy, the linear momentum and the angular momentum of arbitrary fields," Physica **7**(5), 449–474 (1940).
33. B. K. Y. Bliokh, M. A. Alonso, E. A. Ostrovskaya, and A. Aiello, "Angular momenta and spin-orbit interaction of nonparaxial light in free space," Phys. Rev. A **82**(6), 063825 (2010).
34. C. Junge, D. O'Shea, J. Volz, and A. Rauschenbeutel, "Strong coupling between single atoms and nontransversal photons," Phys. Rev. Lett. **110**(21), 213604 (2013).
35. A. Canaguier-Durand and C. Genet, "Transverse spinning of a sphere in a plasmonic field," Phys. Rev. A **89**(3), 033841 (2014).
36. M. Lax, W. H. Louisell, and B. McKnight, "From Maxwell to paraxial wave optics," Phys. Rev. A **11**(4), 1365–1370 (1975).
37. V. D'Ambrosio, F. Baccari, S. Slussarenko, L. Marrucci, and F. Sciarrino, "Arbitrary, direct and deterministic manipulation of vector beams via electrically-tuned q-plates," Sci. Rep. **5**, 7840 (2015).
38. A. M. Belskii and A. P. Khapalyuk, "Internal conical refraction of bounded light beams in biaxial crystals," Opt. Spectrosc. **44**, 436–439 (1978).
39. M. V. Berry, "Conical diffraction asymptotics: fine structure of Poggendorff rings and axial spike," J. Opt. A **6**(4), 289–300 (2004).
40. M. V. Berry, M. R. Jeffrey, and J. G. Lunney, "Conical diffraction: observations and theory," Proc. R. Soc. A **462**(2070), 1629–1642 (2006).
41. V. Peet, "Biaxial crystal as a versatile mode converter," J. Opt. **12**(9), 095706 (2010).
42. V. Peet, "Conical refraction and formation of multiring focal image with Laguerre-Gauss light beams," Opt. Lett. **36**(15), 2913–2915 (2011).
43. C. F. Phelan, D. P. O'Dwyer, Y. P. Rakovich, J. F. Donegan, and J. G. Lunney, "Conical diffraction and Bessel beam formation with a high optical quality biaxial crystal," Opt. Express **17**(15), 12891–12899 (2009).
44. Y. V. Loiko, A. Turpin, T. K. Kalkandjiev, E. U. Rafailov, and J. Mompart, "Generating a three-dimensional dark focus from a single conically refracted light beam," Opt. Lett. **38**(22), 4648–4651 (2013).
45. A. Turpin, Y. Loiko, T. K. Kalkandjiev, H. Tomizawa, and J. Mompart, "On the dual-cone nature of the conical refraction phenomenon," Opt. Lett. **40**(8), 1639–1642 (2015).
46. B. Richards, E. Wolf, "Electromagnetic diffraction in optical systems: structure of the image field in an aplanatic system," Proc. R. Soc. Lond. A Math. Phys. Sci. **253**(1274), 358–379 (1959).
47. M. C. Pujol, M. Rico, C. Zaldo, R. Solé, V. Nikolov, X. Santos, M. Aguiló, and F. Díaz, "Crystalline structure and optical spectroscopy of Er^{3+}-doped $KGd(WO4)_2$ single crystals," Appl. Phys. B **68**(2), 187–197 (1999).

1. Introduction

Linking the classical electromagnetic "spin" with the rotation of the electric and magnetic field vectors about the light propagation direction has constituted a significant step in understanding the nature of the spin angular momentum (SAM) of light [1–5].

In the case of an ideal elliptically polarized plane wave, the degree of circular polarization (helicity) is directly represented by the longitudinal SAM, i.e. the projection of SAM on the wave propagation direction. The transverse component of SAM is equal to zero in this case. The same holds true for freely propagating scalar (i.e. homogeneously polarized) paraxial Gaussian-type beams. As such beams are almost purely transverse with respect to the electromagnetic field components, the direction of their SAMs coincides with the beam axes, i.e. remains longitudinal [3–6].

Nevertheless, even a simple superposition of noncollinear plane waves or scalar paraxial beams does contain a longitudinal projection of the electromagnetic field on the common optical axis and, as a result, may potentially carry transverse SAM. Indeed, Bekshaev *et al.* have shown recently that the interference of two plane waves, or paraxial Gaussian beams, with different states of polarization gives rise to a large transverse SAM [7]. In an analogous manner, a tightly focused superposition of spatially separated beams with carefully tailored individual polarization states can produce transverse SAM in the focal region [8–12].

In their recent work Banzer *et al.* [9] have generated light states with pure transverse SAM by tightly focusing a light field with a specially engineered polarization structure. A polarization converter comprising two quarter-wave plates with orthogonal orientations of their fast axes was utilized to generate spatially separated regions of left- and right-handed circular polarization in the beam of light in the pupil of a high numerical aperture (NA) focusing system. The presence of transverse SAM has been detected in the narrow region near the focal plane along the optical axis where the strong interference between the left- and right-handed circularly polarized light occurred. Under these experimental conditions, the light diffraction at the boundary between the wave plates had a detrimental effect on the beam quality and formation of transverse SAM out of the focal plane.

On the other hand, the state of polarization can vary spatially even in paraxial regime in so called vector beams, formed by superimposing scalar beams with different states of polarization [13,14]. Consequently, the SAM density of vector beams (i.e., SAM associated with the local polarization state) can be distributed non-uniformly. Moreover, vector beams typically contain non-negligible longitudinal components of electromagnetic field when they are focused tightly [15], and thus can potentially carry transverse SAM. The natural representatives of beams with polarization structure resembling that studied by P. Banzer *et al.* [9] are the so-called *full Poincaré beams*, i.e. beams whose spatially variant polarization states span the whole Poincaré sphere [17–20]. In general, these beams can be represented as a superposition of orthogonally polarized modes such as Laguerre-Gauss or Bessel beams with the same frequency and beam waist [14, 21]. As a result, the local polarization of Poincaré beams, which may be linear, elliptical, and circular, varies both azimuthally and radially.

In this work, we propose to realize transverse SAM by tight focusing of a full Poincaré beam comprising two simplest Laguerre-Gauss modes – the LG_{00} and LG_{01} modes with orthogonal linear polarizations. We show that the efficiency of the formation of transverse SAM strongly depends on the NA and shape of the entrance pupil of the focusing system. For a fixed NA the maximum efficiency can be obtained by using an ultrathin annular aperture such that the resulting focused beam is similar to the Poincaré-Bessel beam [14]. Moreover, it appears that the state with a transverse SAM can exist over an extremely long distance along the optical axis. Finally, we show that the desired nontrivial beam structure in the form of a thin ring with variant polarization can be efficiently realized by using the phenomenon of conical refraction in biaxial crystals. Tight focusing of conically refracted light leads to the

formation of a full Poincaré-Bessel beam with a very strong transverse SAM and can provide an additional degree of freedom in optical spanners [22–24] and polarization-sensitive optical manipulation [25,26]. Tightly focused Poincaré-Bessel beams can also have potential applications in laser material processing [27–29], acceleration of charged particles [30], and microscopy [31].

2. Theory

To describe the distribution of SAM density we start from its general definition in Gaussian units ($\varepsilon_0 = \mu_0 = 1$) as [4,5,32,33]:

$$s \propto \mathrm{Im}[(\boldsymbol{E}^* \times \boldsymbol{E}) + (\boldsymbol{H}^* \times \boldsymbol{H})]. \tag{1}$$

Here, we note that even though for plane waves, as well as for paraxial beams, there is no difference between the electric and magnetic representation of SAM [4], in general case the electric part is different from its magnetic counterpart. In spite of the fact that the most common materials predominantly react to the local electric field when SAM is measured [34,35], generally the magnetic contribution to the SAM density cannot be ignored. The SAM density (1) can be rewritten explicitly in the Cartesian coordinates as:

$$
\begin{aligned}
\boldsymbol{s}_E &\propto \mathrm{Im}[(E_y^* E_z)\boldsymbol{e}_x + (E_z^* E_x)\boldsymbol{e}_y + (E_x^* E_y)\boldsymbol{e}_z], \\
\boldsymbol{s}_H &\propto \mathrm{Im}[(H_y^* H_z)\boldsymbol{e}_x + (H_z^* H_x)\boldsymbol{e}_y + (H_x^* H_y)\boldsymbol{e}_z],
\end{aligned}
\tag{2}
$$

where $\boldsymbol{e}_x$ and $\boldsymbol{e}_y$ are Cartesian unit vectors, $E_{x,y,z}$ and $H_{x,y,z}$ are the x-, y- and z-components of the electric and magnetic vectors of the light field, respectively.

In the paraxial approximation, the electromagnetic of a monochromatic light beam propagating along the positive direction of the z-axis can be expressed as a superposition of purely orthogonally polarized components $\boldsymbol{U}(x,y,z)e^{ikz}$ characterized by the slow varying complex amplitude [36]:

$$\boldsymbol{U} = U_x(x,y,z)\boldsymbol{e}_x + U_y(x,y,z)\boldsymbol{e}_y \tag{3}$$

In terms of the complex amplitude $\boldsymbol{U}$, the paraxial electric and magnetic fields are given by [5,36]:

$$
\begin{aligned}
\boldsymbol{E} &= \left[\boldsymbol{U} + ik^{-1}(\nabla_\perp \cdot \boldsymbol{U})\boldsymbol{e}_z\right]e^{ikz}, \\
\boldsymbol{H} &= \left[(\boldsymbol{e}_z \times \boldsymbol{U}) + ik^{-1}(\nabla_\perp \cdot (\boldsymbol{e}_z \times \boldsymbol{U})\boldsymbol{e}_z\right]e^{ikz}.
\end{aligned}
\tag{4}
$$

In the zero-order paraxial approximation, the second terms appearing in the brackets in Eq. (4) are neglected and the energy flow density (EFD) and the SAM density are therefore determined only by the transverse components of the field. The intensity of the beam is nothing else but EFD, while the total power in the beam is $W = c/(8\pi)\int \boldsymbol{U} \cdot \boldsymbol{U}^* d\rho^2$, where c is the speed of light in vacuum.

Here, we consider a paraxial Poincaré beam in the pupil plane $z = 0$ of the focusing objective. The Poincaré beam is represented by a superposition of an x-polarized LG$_{00}$ mode and a y-polarized LG$_{01}$ mode (i.e., single charge optical vortex), each of which has power W and beam waist radius w_0 [21]. In this case, the scalar complex amplitudes U_x and U_y in polar coordinates (ρ, φ, z) are:

$$
\begin{aligned}
U_x(\rho, z = 0) &\equiv u_x(\rho) = 4\sqrt{W/(w_0^2 c)}\exp(-\rho^2/w_0^2), \\
U_y(\rho, \varphi, z = 0) &\equiv u_y(\rho)e^{-i\varphi} = 4\sqrt{2W/(w_0^2 c)}(\rho/w_0)\exp(-\rho^2/w_0^2)e^{-i\varphi},
\end{aligned}
\tag{5}
$$

Such a beam can be synthesized, for instance, with the help of a spatial light modulator combined with a Mach-Zender interferometer [21], by using q-plates [37], or by employing the phenomenon of conical refraction in biaxial crystals [38–45]. Figure 1(a) shows the intensity and polarization distribution in the cross section of the beam.

Below we will discuss the focusing of the above Poincaré beam with a lens of focal length f and numerical aperture NA. The complex amplitude of the field in the pupil plane of the lens can be presented as: $U(\theta, \varphi) = u_x(\theta)\hat{e}_x + u_y(\theta)e^{-i\varphi}\hat{e}_y$, where

$$u_x(\theta) = 4\sqrt{W/c}\,\frac{1}{fNAw_f}\exp\{-\sin^2\theta/(NAw_f)^2\},$$

$$u_y(\theta) = 4\sqrt{2W/c}\,\frac{\sin\theta}{fNA^2w_f^2}\exp[-\sin^2\theta/(NAw_f)^2]e^{-i\varphi}.,$$

(6)

In the above equations we expressed the radial coordinate ρ through the focal length f and focal angle θ as $\rho = f\sin\theta$ and normalized the beam waist w_0 to the outer radius of the focusing lens, i.e., $w_f = w_0/(NAf)$ [see Fig. 1(b)].

The electric and magnetic field components of the incident Poincaré beam can be written as:

$$E_{in}(\theta, \varphi) = \left[u_x(\theta)e_x + u_y(\theta)e^{-i\varphi}e_y\right]e^{ikz},$$

$$H_{in}(\theta, \varphi) = [-u_y(\theta)e^{-i\varphi}e_x + u_x(\theta)e_y]e^{ikz}.$$
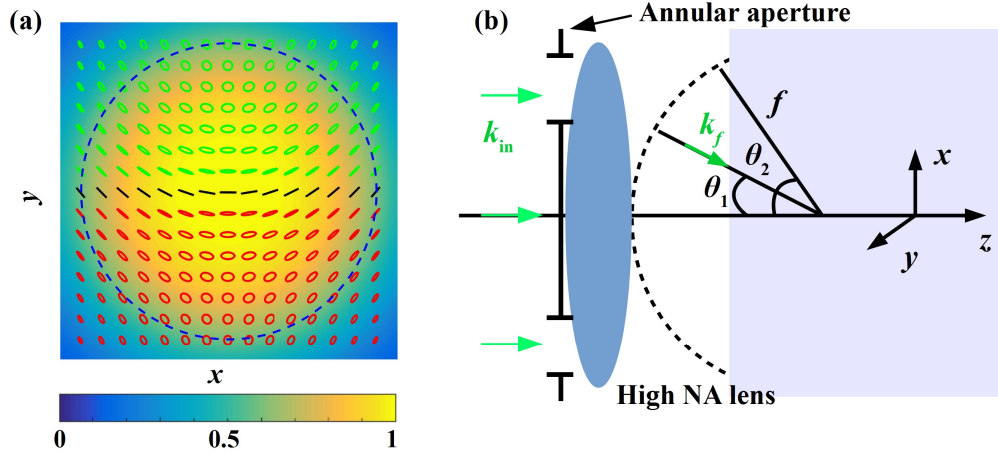
(7)

Fig. 1. (a) The polarization and intensity distribution of the full Poincaré beam given by Eq. (7) for $w_f = 1.30$. Right-handed circular, linear and left-handed circular polarization states are shown in red, green, and black, respectively. The blue circle represents polarization states along the meridian of the Poincaré sphere. (b) Schematic of tight focusing with a high NA lens.

We would like to emphasize that the beam (7) is purely paraxial ($w_0 \gg \lambda$) in the plane $z = 0$ and the electric and magnetic fields are purely transverse. Therefore, the direction of its SAM coincides with the beam axis, i.e. the z-axis.

The electric and magnetic field components of the beam (7) in the focus of the lens can be calculated by using the Richards-Wolf theory [46] as $E = E_x e_x + E_y e_y + E_z e_z$ and $H = H_x e_x + H_y e_y + H_z e_z$, where each component is, respectively:

$$E_x = [I_x^0 + \cos 2\phi K_x^2 - (ie^{i\phi}K_y^1 - ie^{-i3\phi}K_y^{-3})/2],$$
$$E_y = [\sin 2\phi K_x^2 + e^{-i\phi}I_y^{-1} - (e^{i\phi}K_x^1 + e^{-i3\phi}K_y^{-3})/2], \qquad (8)$$
$$E_z = [2\cos\phi L_x^1 - iL_y^0 + ie^{-i2\phi}L_y^{-2}],$$

and

$$H_x = [\sin 2\phi K_x^2 - e^{-i\phi}I_y^{-1} - (e^{i\phi}K_x^1 + e^{-i3\phi}K_y^{-3})/2],$$
$$H_y = [I_x^0 - \cos 2\phi K_x^2 + (ie^{i\phi}K_y^1 - ie^{-i3\phi}K_y^{-3})/2], \qquad (9)$$
$$H_z = [2\sin\phi L_x^1 - L_y^0 - e^{-i2\phi}L_y^{-2}],$$

In Eqs. (8) and (9)

$$I_{x,y}^n = i^n C \int_{\theta_1}^{\theta_2} \sqrt{\cos\theta} \sin\theta J_n(k_0 r \sin\theta) e^{ik_0 z\cos\theta}(\cos\theta+1)u_{x,y}(\theta)d\theta,$$

$$K_{x,y}^n = i^n C \int_{\theta_1}^{\theta_2} \sqrt{\cos\theta} \sin\theta J_n(k_0 r \sin\theta) e^{ik_0 z\cos\theta}(\cos\theta-1)u_{x,y}(\theta)d\theta,$$

$$L_{x,y}^n = i^n C \int_{\theta_1}^{\theta_2} \sqrt{\cos\theta} \sin^2\theta J_n(k_0 r \sin\theta) e^{ik_0 z\cos\theta}u_{x,y}(\theta)d\theta,$$

where C is the normalization factor, $J_n(x)$ is the Bessel function of the first kind of order n, and θ_1, and θ_2 are determined by the annular aperture, as shown in Fig. 1(b).

By integrating and normalizing the SAM density over the xy-plane we get the average SAM per photon, $S = \int s\,dxdy / \int [|E|^2 + |H|^2]dxdy$.

The normalized average SAM can be alternatively obtained by the quantum-operator formalism $S = \langle U^\sigma | \sigma\kappa | U^\sigma \rangle / \langle U^\sigma \| U^\sigma \rangle$ or $S = \sum_\sigma \sigma \int |U^\sigma|^2 \kappa d^2\kappa_\perp / \sum_\sigma \int |U^\sigma|^2 d^2\kappa_\perp$

described in Ref [33], where $\sigma = 2^{-1/2}(e_x + i\sigma e_y)$ and $\kappa = \sin\theta\cos\varphi e_x + \sin\theta\sin\varphi e_y + \cos\theta e_z$ are a unit circular vector and a unit spherical vectors respectively, $\sigma = \pm 1$ and sign + (–) corresponds to right (left) circular polarization. Our initial conditions give $U^\sigma = [u_x(\theta) - \sigma i u_y(\theta)e^{-i\varphi}]\sigma$, and then the normalized average can be finally found as:

$$S = \frac{\int_{\theta_1}^{\theta_2} u_x u_y \sin^2\theta d\theta}{\int_{\theta_1}^{\theta_2}[u_x^2 + u_y^2]\sin\theta d\theta} \hat{e}_y. \qquad (10)$$

From the Eq. (10) it is clearly seen that the longitudinal component of the average SAM vanishes and, therefore, the average SAM is purely transverse.

Figure 2 shows how the average transverse SAM depends on θ_1 and the normalized beam waist w_f. The numerical simulations are performed using Eq. (10) with NA = 0.95 and θ_2 = 71.8°. As w_f increases, the average transverse SAM first grows, reaches its maximum value, and then gradually declines. On the other hand, it always monotonically increases with θ_1. The normalized beam waist w_f required to achieve the maximum average transverse SAM varies slightly with θ_1, from 1.30 at $\theta_1 = 0°$ to $\sqrt{2}$ at $\theta_1 \rightarrow 71.8°$. When $\theta_1 \rightarrow \theta_2$, which corresponds to the situation when the annular aperture is infinitely narrow, and $w_f = \sqrt{2}$, the average transverse SAM takes on its maximum value of 0.475. Interestingly, in this limit the focal field has the form of a Bessel-Poincaré beam [14] consisting of J_0 and J_1 beams.
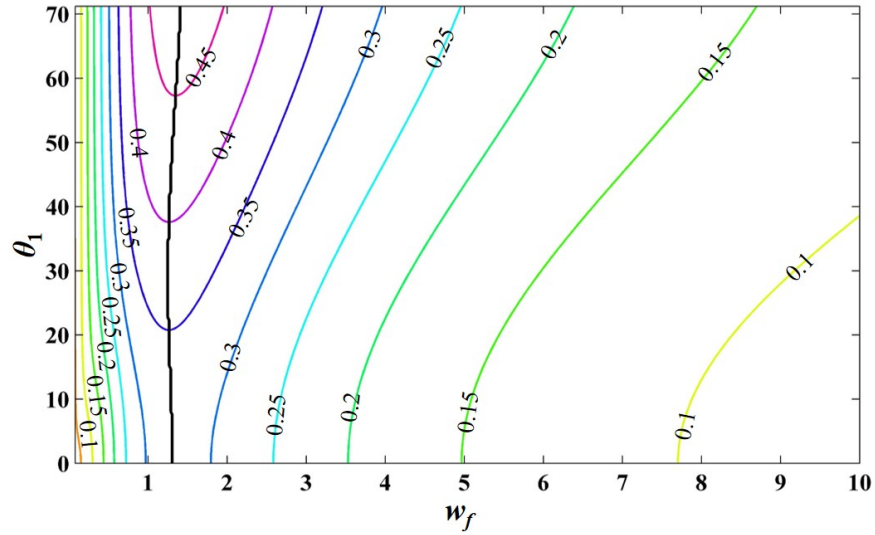
Fig. 2. Average transverse SAM [S_y]on the minimum focal angle θ_l and the normalized beam waist w_f. The black line indicates the maximum value of SAM.

In Figs. 3 and 4 we plot the transverse distributions of total intensity and SAM density (s) for the cases with ($\theta_l = 64°$) and without ($\theta_l = 0°$) an annular aperture, when $w_f = 1.3$. It is clear that the presence of a narrow annular aperture leads to smaller focal spot size. At the same time however, it results in appearance of diffraction rings in the spatial intensity distribution. Moreover, in both cases the focal spots exhibit a small transverse shift toward the negative x direction, which corresponds to the emergent nonzero y-component of average SAM. Although the y-component of SAM density s_y takes negative and positive values, the positive s_y prevails leading to the nonzero average SAM, $S_y = 0.315$ for $\theta_l = 0°$, and up to 0.463 for $\theta_l = 64°$. The increase of average SAM results from the filtering out low spatial frequencies of the focal field. In both cases the x and z components of SAM densities are small, and their alternating sign results in zero average SAM.
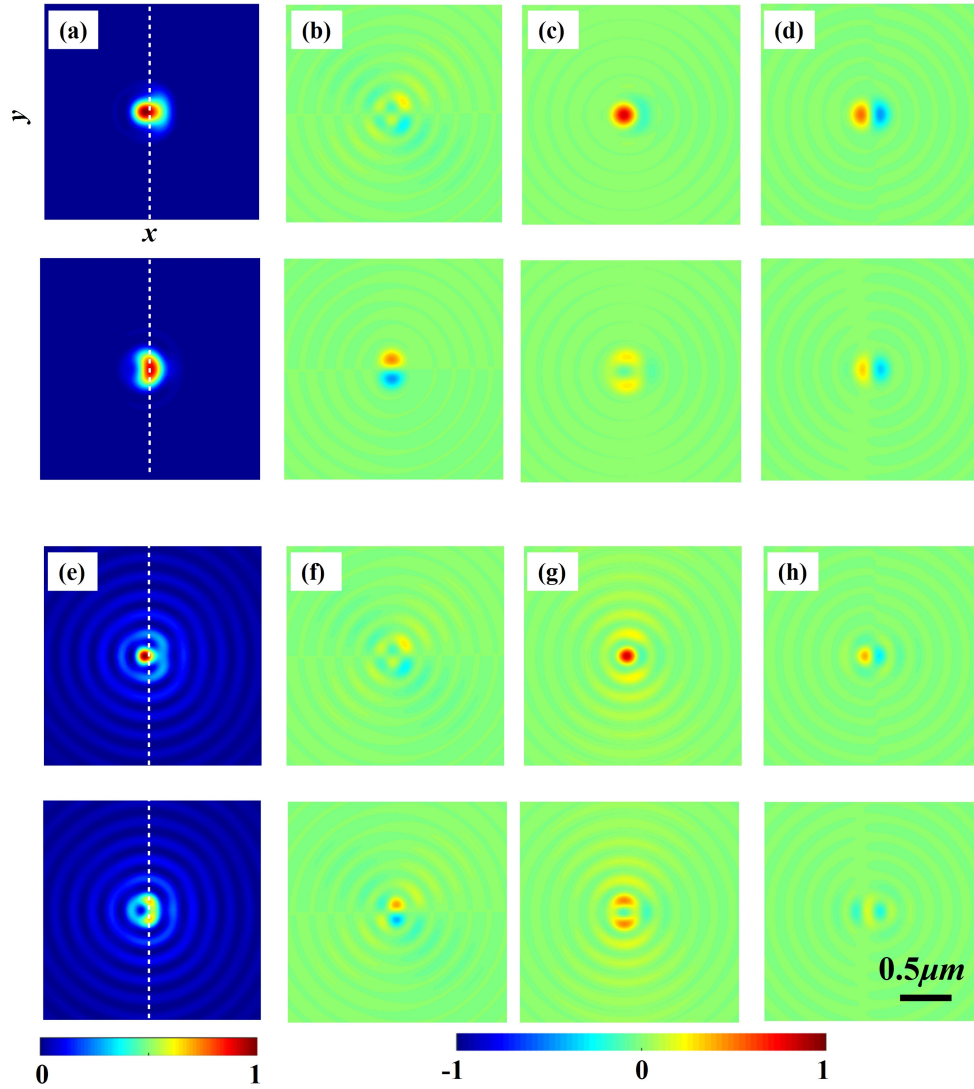
Fig. 3. The distributions of electric **EE***(first and third rows) and magnetic **HH*** (second and forth rows) parts of field energy (a,e) and the SAM densities [s_x (b,f), s_y (c,g), and s_z (d,h)] of focal field in the focal plane for $\theta_1 = 0°$ (a-d) and $\theta_1 = 64°$ (e-h), when $w_f = 1.30$. All quantities are normalized to the maximum electric field energy.

It is worth mentioning that not only does the geometry of annular aperture determine the magnitude of the transverse SAM, but it also has a dramatic effect on the size of the region along the optical axis when the SAM is nonzero. This is illustrated in Fig. 4, which depicts numerically calculated longitudinal (along the propagation axis) cross-section of distribution patterns of electric (left column) and magnetic (right column) parts of field energy and the SAM density in the focal area of high numerical aperture lens (NA = 0.95). Figures 4(a)-4(d) and 4(e)-4(h) correspond to two different inner apertures of $\theta_1 = 0°$ and $\theta_1 = 64°$, respectively. It is evident that for the fully open aperture ($\theta_1 = 0°$) the nonzero transverse SAM is confined to a narrow (submicron) region near the focal plane, while it significantly expands (up to few microns) when the aperture is very narrow ($\theta_1 = 64°$). This property is of great importance for practical application of the transverse SAM.
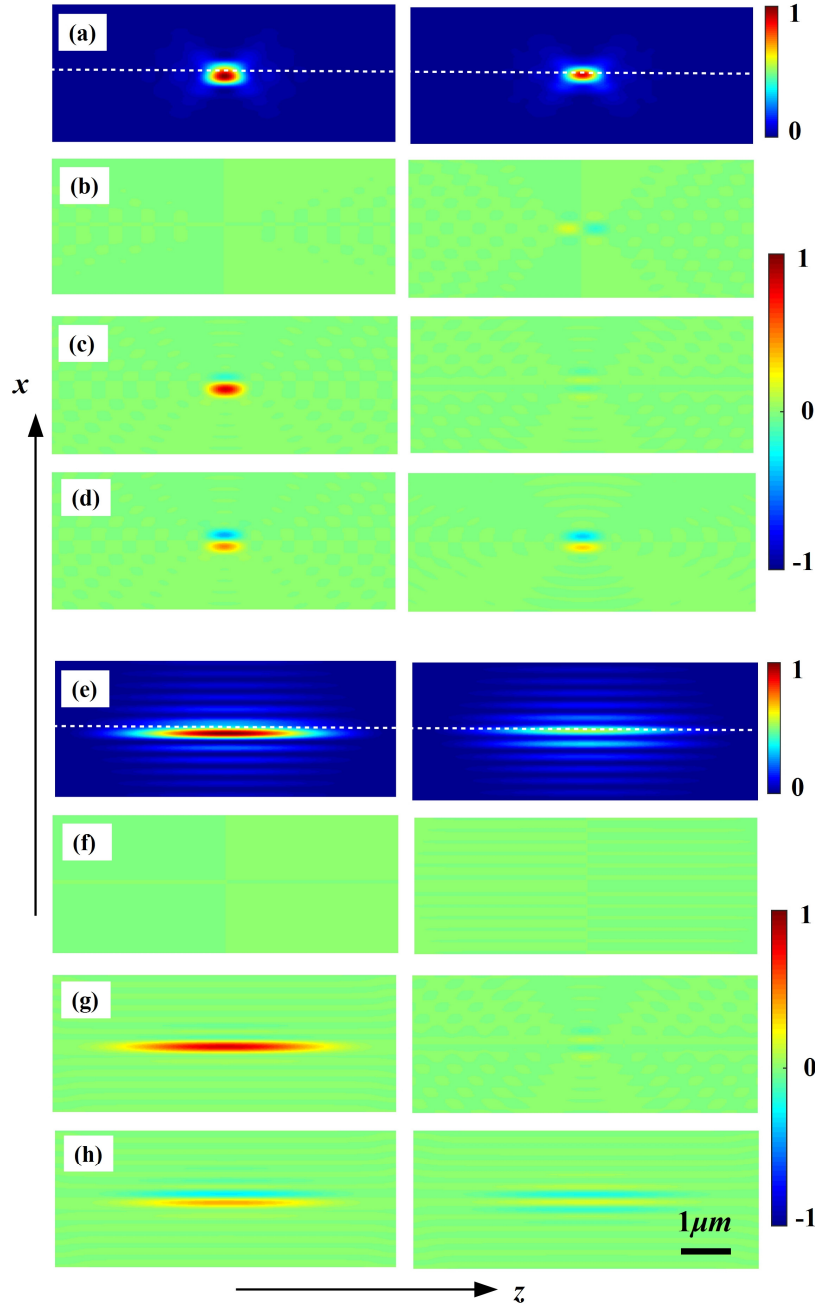
Fig. 4. The distributions of electric **EE*** (left column) and magnetic **HH*** (right column) parts of field energy (a,e) and the SAM densities [s_x (b,f), s_y (c,g), and s_z (d,h)] of focal field in xz plane for $\theta_1 = 0°$ (a-d) and $\theta_1 = 64°$ (e-h),, when $w_f = 1.30$. All quantities are normalized to the maximum electric field energy. The size of the figures are $5\mu m \times 2\mu m$

Although adding a narrow annular aperture can lead to the creation of a high average transverse SAM in the focal field, the energy efficiency of this approach is very low. Fortunately, the narrow ring-shaped intensity pattern with anti-symmetrically distributed polarization can be easily and efficiently produced via spin-orbit coupling in the process of

conical refraction (CR) which takes place in propagation of optical beams along an optical axis of biaxial crystal (BC) [38–45].

3. Formation of states with SAM via conical refraction

The optical field distribution corresponding to Eq. (7) of the full Poincaré beam can be formed experimentally by employing the conical refraction phenomenon inside a biaxial crystal. Moreover, it is well known that CR can produce a sharp rings of intensity in the focal plane if the light is focused through the crystal [38–40]. The ring-shaped intensity distribution together with the required polarization state allow one to avoid formation of multiple rings caused by light diffraction on the annular aperture, and subsequently limiting the efficiency of the transverse SAM generation process.

In order to produce the required ring-shaped optical field distribution, the first step is to focus the initial circularly polarized paraxial Gaussian beam in the biaxial crystal along one of its optic axes (here z). The complex amplitude $\mathbf{U}^{in}$ of this input beam is:

$$\mathbf{U}^{in} = 4\sqrt{W/c}\,\frac{1}{w_0\xi(z)}\exp\left(-\frac{\rho^2}{w_0^2\xi(z)}\right)\boldsymbol{\sigma}^{\pm}, \tag{11}$$

where $\xi(Z) = 1 + iz/z_0$, $z_0 = kw_0^2/2$ is the Rayleigh length of the beam, $\boldsymbol{\sigma}^{\pm} = 2^{-1/2}(\mathbf{e}_x + i\sigma\,\mathbf{e}_y)$ is a unit circular vector, $\sigma = \pm 1$ and sign + and – corresponds to right hand and left hand states of polarization respectively, and k is the wave number.

The conical refraction phenomena in the biaxial crystal is characterized by the half intersection angle of the two ellipsoids of refractive indices or conicity parameter, $\alpha = \sqrt{\left(n_2^2 - n_1^2\right)\left(n_3^2 - n_2^2\right)/n_2^2}$, where one assumed $n_1 < n_2 < n_3$ [38, 39]. When the length of the crystal along its optical axis is l, it is convenient to introduce the parameter $R_0 = \alpha l$, that has simple geometrical optics interpretation as a ring radius of the conical refraction pattern behind the crystal. When the fundamental Gaussian beam propagates along the optical axis, the resulting distribution of the light field strongly depends on both crystal and beam parameters, such as R_0 and waist radius w_0 of the input beam in the vacuum. Hence, the use of common parameters $\rho_0 = R_0/w_0$ and $\rho_1 = \rho/w_0$ simplifies description of the light beam after the crystal. Moreover, for convenience in an analytical description, we will express the longitudinal position with respect to a new origin located at $z = l(1 - 1/n_2)$ [40].

According to the Belsky-Khapalyuk-Berry theory [39, 40] and as confirmed by other authors [41–45], for the circularly polarized input Gaussian beam the complex amplitude corresponding to both electric field and magnetic field of output beams can be written as:

$$\mathbf{U} = \left(B_0\boldsymbol{\sigma}^{\pm} + B_1 e^{\pm i\varphi}\boldsymbol{\sigma}^{\mp}\right), \tag{12}$$

where B_0 and B_1 are given as:

$$\begin{aligned}
B_0 &= \frac{1}{2\pi}\int_0^{\infty}\eta a(\eta)e^{-iz\eta^2/4z_0}\cos(\eta\rho_0)J_0(\eta\rho_1)d\eta, \\
B_1 &= \frac{1}{2\pi}\int_0^{\infty}\eta a(\eta)e^{-iz\eta^2/4z_0}\sin(\eta\rho_0)J_1(\eta\rho_1)d\eta,
\end{aligned} \tag{13}$$

Here η is the modulus of transverse wave vector $\eta = |\mathbf{k}_{\perp}|k_0 w_0$, measured in units of $1/w_0$, $a(\eta)$ denotes the spatial Fourier spectrum of an incident beam. For a Gaussian input beam $G(\rho_1, 0) = \exp\left(-\rho_1^2\right)$ one gets $a(\eta) = \pi\exp(-\eta^2/4)$ [40].

The first term in Eq. (12) represents a topologically uniform circularly polarized beam, while the second one is orthogonally polarized single charge optical vortex. The handedness of the circular polarization of the first beam coincides with that of the input beam while the vortex-like component's is opposite. Moreover, the sign of the topological charge of the second beam coincides with the sign of the initial circular polarization.

While the resulting light intensity distribution is spatially nonuniform, it is symmetric with respect to the focal plane $z = 0$. In particular, when the parameter $\rho_0 > 1$ the central axial intensity peak splits up into a pair of separate bright spots (Raman spots) symmetrically located on both sides of $z = 0$ where the light intensity acquires minimum. For $\rho_0 \gg 1$ this intensity minimum is of the order of $1/\rho_0^2$ [40]. The spatial intensity pattern at the focal plane $z = 0$ has a form of a pair of concentric rings separated by a dark (Poggendorff) ring. The two bright rings represent two conical fields – one diverging from and the second converging towards corresponding Raman spots. Therefore, in order to create the uniform ring of light intensity distribution, one starts with focusing the circularly polarized Gaussian inside the crystal and ensuring that $\rho_0 \gg 1$.
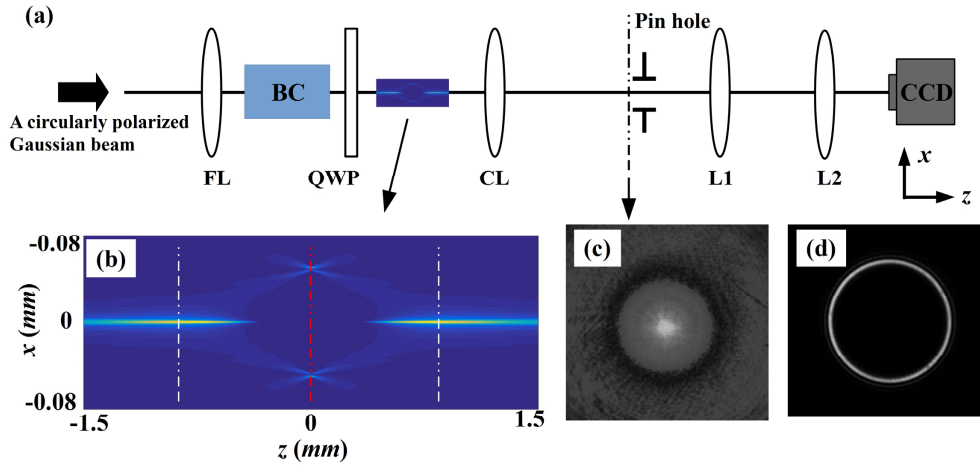

Fig. 5. The schematic for the creation of narrow ring-shaped intensity pattern with anti-symmetrically distributed Stokes parameter. A circularly polarized Gaussian beam is focused by the focal lens (FL) with NA = 0.3 into BC. After collimated by a collimating lens (CL) (NA = 0.65), the conically diffracted beam is filtered by a pin hole. The ring-shaped intensity pattern is obtained in the focal plane of lens 1 (L1). The lens 2 (L2) and CCD forms an image system. The QWP convert the polarization into the desired one. (b) The intensity distribution of total intensity near the image focal plane, where red line and two white lines indicate the focal and front and back spots planes, respectively. Two white vertical lines indicate positions of two Raman spots. (c, d) The experimentally measured intensity distributions in front of pin hole (c) and in the CCD plane (d).

As discussed earlier, for the formation of states with high transverse SAM, the ring-shaped field should carry anti-symmetric distribution of polarization in the form (7). It appears that for the circularly polarized input beam, the polarization of the CR field is linear and its orientation varies azimuthally along the ring. However, when such a state of polarization is converted by a quarter wave plate (QWP) whose fast axis forms an angle φ_0 with the x-axis and whose corresponding transmission matrix is:

$$T = \frac{\sqrt{2}}{2}\begin{bmatrix} 1 - i\cos 2\varphi_0 & -i\sin 2\varphi_0 \\ -i\sin 2\varphi_0 & 1 + i\cos 2\varphi_0 \end{bmatrix},$$

(14)

the resulting state of the polarization has exactly the required anti-symmetric spatial distribution. After the conversion the complex amplitude distribution reads:

$$U = \sqrt{1/2}\{[B_0 - iB_1 e^{\pm i(\varphi - 2\varphi_0)}]\boldsymbol{\sigma}^{\pm} + [-iB_0 e^{\pm i2\varphi_0} + B_1 e^{\pm i\varphi}]\boldsymbol{\sigma}^{\mp}\}. \tag{15}$$

In an experimental setup we consider right handed circularly polarized Gaussian beam $\sigma = +1$ propagating along the optic axis of the KGD(WO$_4$)$_2$ biaxial crystal of thickness $l = 2.8$mm as shown in the Fig. 5. The principal refractive indices of the crystal at 632 nm wavelength are $n_1 = 2.013$, $n_2 = 2.045$, $n_3 = 2.086$, respectively [47]. The beam is focused into the BC by a lens (FL) with NA = 0.3. In these focusing conditions the beam waist parameter is $w_0 \sim 1.3 \mu$m. After the crystal the beam is converted by QWP to obtain the required polarization distribution (15) in the focal imaging plane. The conically refracted field forms an optical bottle near the image focal plane. In the focal plane ($z = 0$), the cross-section of the bottle has a form of double bright rings, separated by a dark Poggendorff ring.
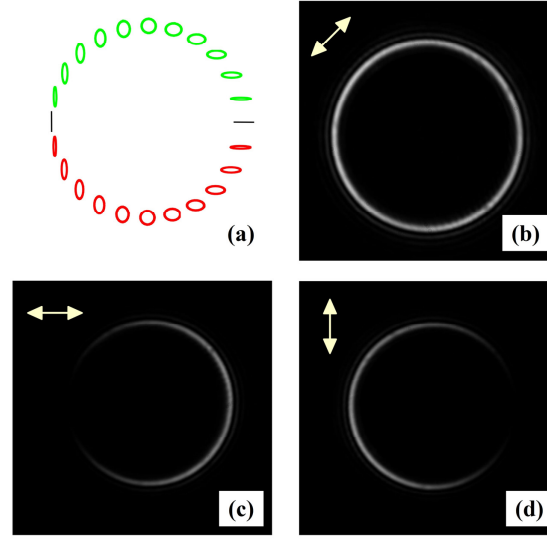

Fig. 6. (a) The polarization states of conically diffracted fields after QWP with $\varphi_0 = \pi/2$. The red, green, and pink lines represent $s_3 > 0$, $s_3 < 0$, and $s_3 = 0$, respectively. (b~c) The experimentally recorded intensity distributions of the CR ring structure after a polarizer with diagonal (b), horizontal (c), and vertical (d) directions.

To obtain a required single narrow ring-shaped intensity pattern, one needs to remove one of the bright rings. This can be done by placing a small aperture at either the front or back Raman's spot allowing only one of the conical fields to pass through. Experimentally, we first collimate the conically diffracted beam with a high NA (0.65) lens (CL), and then put the pinhole at the rear Raman's spot, whose intensity distribution is shown in Fig. 5(c). After passing through another lens (L1), the emerging beam forms the desired ring-shaped intensity pattern appearing in the focal plane, which is imaged by a combination of lens (L2) and a CCD camera. This ring-shaped intensity pattern is shown in Fig. 5(d). The measured ratio of radius of the ring to its width at the $1/e^2$ intensity level is about 20. In comparison, the corresponding ratio for the full Poincaré beam with the annular aperture of $\theta_1 = 64°$ is 18.5. Therefore, one may expect the average transverse SAM generated by using the ring-shaped field obtained in CR will be close to that of the full Poincaré beam. Moreover, it turns out that conversion efficiency in the former case can be as high as 50%.

Figure 6(a) depicts calculated distribution of polarization states along the ring for $\varphi_0 = \pi/2$. This polarization pattern is observed experimentally by propagating the beam through a linear

polarizer. The transmitted field distribution, for various orientation of the polarizer is shown in Figs. 6(b)-6(d) and clearly validates the polarization distributions in Fig. 6(a). It should be noted that the distribution of the polarization pattern also rotates linearly with φ_0. Therefore, one can control the polarization by tuning the fast axis of QWP, and thus the direction of transverse SAM.

The above discussion shows that the average transverse SAM by a conically refracted beam can reach a value close to the theoretical limit 0.5NA (= 0.46) for a full Poincaré beam. This value should be compared with that reported earlier by Neugebauer *et. al.* [10]. In their work the transverse SAM was formed with the aid of segmented states of polarization such that the light field in the upper (lower) half space carried right-handed (left-handed) circular polarization. This state was realized by passing a linearly polarized TEM_{10} (Hermite-Gauss) mode through a segmented quarter wave plate. The subsequent focusing by a high NA lens led to a non-zero transverse component of average SAM in the focal plane. Using the same NA = 0.95, the average transverse SAM per photon could be estimated to reach in that case a value of 0.27 which is significantly smaller than that generated by the full Poincaré beam considered above.

Therefore, conical refraction allows one to efficiently generate a Poincaré beam, which should yield high average transverse SAM when tightly focused. The experimental verification of this high transverse SAM is a challenging task and will be a subject of future work. In principle, this could be achieved by using recently demonstrated a nanoprobing technique based on the directional far-field emission of a transversely spinning dipole located on a dielectric interface [9].

4. Conclusions

In conclusion, we have demonstrated that the full Poincaré beam in linear polarization basis is a suitable candidate for efficient generation of transverse spin angular momentum. The average transverse SAM can be controlled by varying the spatial spectrum of the incoming field and attains maximum value of 0.5NA per photon which, for typical value of NA = 0.95 is significantly higher than that reported earlier. Moreover, we have shown that similar highly efficient generation of transverse SAM can be achieved by employing the field generated in conical refraction of light. In general, it appears that the high transverse SAM combined with small focal spot make the full Poincaré beams promising candidates for applications involving laser-matter interaction with light beam carrying transverse spin angular momentum.

Acknowledgments